Interfacial Protection of Topological Surface States in Ultrathin Sb Films

Guang Bian,[1,2] Xiaoxiong Wang,[1,2,3] Yang Liu,[1,2] T. Miller,[1,2] and T.-C. Chiang[1,2]

[1]*Department of Physics, University of Illinois at Urbana-Champaign, 1110 West Green Street, Urbana, Illinois 61801-3080, USA*

[2]*Frederick Seitz Materials Research Laboratory, University of Illinois at Urbana-Champaign, 104 South Goodwin Avenue, Urbana, Illinois 61801-2902, USA*

[3]*College of Science, Nanjing University of Science and Technology, Nanjing 210094, China*

(Received 23 January 2012; published 25 April 2012)

Spin-polarized gapless surface states in topological insulators form chiral Dirac cones. When such materials are reduced to thin films, the Dirac states on the two faces of the film can overlap and couple by quantum tunneling, resulting in a thickness-dependent insulating gap at the Dirac point. Calculations for a freestanding Sb film with a thickness of four atomic bilayers yield a gap of 36 meV, yet angle-resolved photoemission measurements of a film grown on Si(111) reveal no gap formation. The surprisingly robust Dirac cone is explained by calculations in terms of interfacial interaction.

DOI: 10.1103/PhysRevLett.108.176401 PACS numbers: 71.70.Ej, 73.20.At, 73.21.Fg, 79.60.Dp

Topological insulators have attracted much interest because their gapless surface states carry a surface spin current, which can be utilized for spintronic and quantum computation applications [1,2]. These states form Dirac cones with a chiral spin structure as a result of the Rashba interaction [3]. For practical device applications, thin films are the standard platform for massive device integration. However, when topological films become ultrathin, the surface states on the two faces of the film can overlap and interact by quantum tunneling of the surface electrons between the two faces. The coupling breaks the degeneracy at the Dirac point, resulting in a gap [4,5]. This gap precludes electrical transport and can be detrimental to device performance, but it is a subject of great interest in connection with the search for Majorana states and other exotic emerging properties [6]. The size of the gap and the underlying interaction are issues of central importance in the physics and applications of topological films, which are the subject matters of the present study of ultrathin Sb(111) films.

Bulk Sb is semimetallic with a negative band gap and a nontrivial topological order [7]. The Sb(111) surface supports a single pair of Rashba-split surface states that span the semimetallic gap with a Dirac cone at the zone center. The simplicity of the electronic structure makes Sb(111) an ideal model system, on which a number of studies have been performed [8–11]. Films of Sb(111) consist of a stack of bilayers (BL), each of which resembles a buckled graphene sheet [12]. As the Sb films become thinner, the semimetallic gap widens. Our first-principles calculations show that the gap at a film thickness of 4 BL becomes slightly positive [13], making the system insulating in the bulk, a desirable feature for transport applications. However, the same calculation shows a tunneling-induced gap of 36 meV at the Dirac point of the surface states, an undesirable result. Surprisingly, angle-resolved photoemission spectroscopy (ARPES) measurements of a 4-BL film grown on Si(111) reveal no such gap at the Dirac point, even though the rest of the experimental band structure appears very similar to the calculated one. The observed robust gapless Dirac cone is very promising for applications. The puzzling difference between experiment and calculation is explained by additional model calculations taking into account of the substrate.

Our ARPES measurements were performed at the Synchrotron Radiation Center of the University of Wisconsin-Madison. We employed a Bi-terminated Si(111)-$\sqrt{3} \times \sqrt{3} - R30°$ surface [14,15] as the substrate, which supports growth of ultrasmooth Sb films under appropriate conditions [12]. By contrast, growth of Sb directly on Si(111) $-$ (7×7), without the Bi interfactant, yields inferior films. The sample was kept at 60 K during the ARPES measurements. Our first-principles calculations were performed using the ABINIT code [16,17] based on a relativistic local-density approximation, HGH-type pseudopotentials [18], and a plane-wave basis set.

Figure 1(a) presents calculated band structures of freestanding Sb films at various thicknesses in the range of 1–10 BL along the $\bar{\Gamma} - \bar{M}$ direction. The shaded areas indicate the projected bulk band regions, and states within the bulk gap are of surface character. The spin-split surface states begin to appear at a thickness of 2 BL, but there is a fairly large tunneling-induced gap of 86 meV at $\bar{\Gamma}$. This gap diminishes as the film thickness increases and essentially vanishes at $\sim$8 BL when the gap becomes smaller than thermal broadening. The calculated gap ΔE as a function of thickness is shown in Figs. 1(b) and 1(c) using linear and logarithmic scales, respectively. The decay of the gap beyond above about 6 BL is exponential; a fit to the asymptotic behavior yields a decay length of about 1.1 BL, which characterizes the spatial extent of the surface state wave function. The calculated plane-averaged

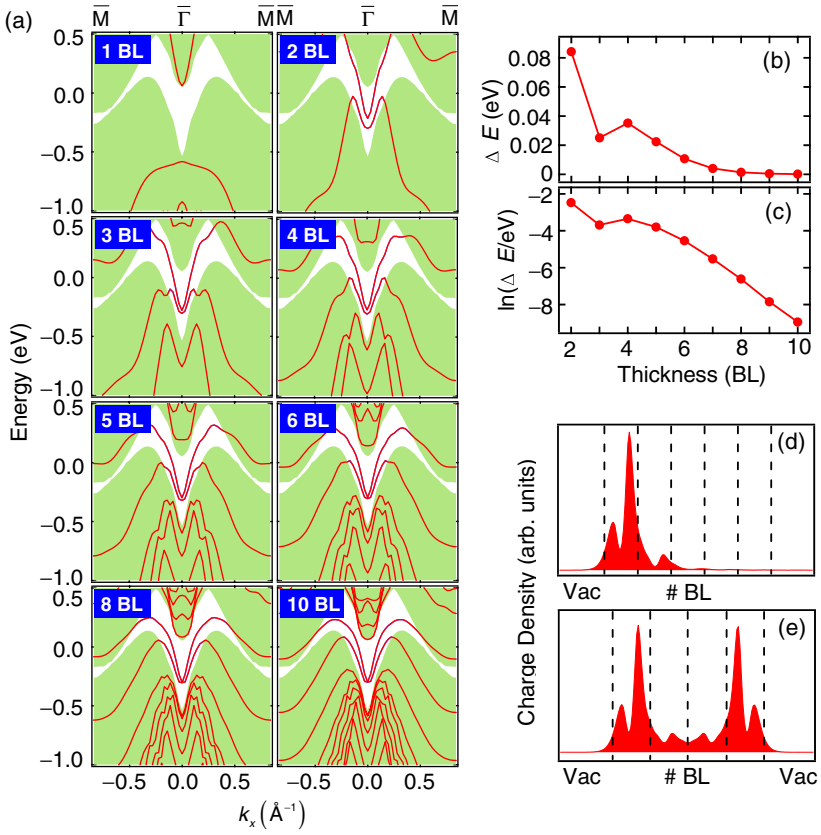

FIG. 1 (color online). (a) Band structure of Sb(111) films of various thicknesses. The shaded areas indicate projected bulk band regions. (b) Calculated energy gap ΔE and (c) logarithmic gap $\ln(\Delta E)$ at $\bar{\Gamma}$ as a function of film thickness. (d) Plane-averaged charge density of the lower surface state at $\bar{\Gamma}$ as a function of distance from the surface for a thick film. The vertical dashed lines indicate the bilayers. (e) Same for a 4-BL film.

charge densities of the lower surface state at the zone center for a thick Sb(111) film and a 4-BL film are shown in Figs. 1(d) and 1(e), respectively. The surface state is mostly localized within the top BL. The small tail allows the surface states associated with the two faces of the 4-BL film to overlap, giving rise to the gap. The other bands in Fig. 1(a) are quantum-well states in the film [12,19]. Unlike the surface states, the quantum-well states are spin degenerate. Another important distinction is that the quantum-well bands become more numerous as the film becomes thicker.

ARPES mapping of the band structure of a 4-BL Sb film is presented in Fig. 2(a). The band dispersions are in fairly good accord with calculated ones presented in Fig. 2(b) for a freestanding 4-BL film. The data confirm the atomic-level uniformity of the film; any significant admixture of 3- or 5-BL patches would give rise to additional quantum-well bands. Similar comparison between experiment and theory for a 20-BL film is presented in Figs. 2(c) and 2(d). The surface states are well resolved, but the dense set of quantum-well states at low energies are not. Despite the overall similarity, the experiment and theory do differ in some details. Shown in Fig. 2(e) is a close-up view of the experimental spin-split surface bands near the zone center for the 4-BL film; the data contrast has been enhanced by taking the second derivative in energy. The corresponding theoretical bands are shown in Fig. 2(f), with the bands suitably broadened to simulate the data. The gap at the zone center, 36 meV in the calculation, is absent in the data. The theoretical dispersion relations have noticeably higher energies.

It is interesting to note that prior studies of related systems such as Bi_2Se_3 thin films have shown convincingly the presence of tunneling-induced gaps at small film thicknesses [20]. Our observation here represents the first clear-cut case of a zero gap at a film thickness where a sizeable gap is predicted. The difference can be attributed to the boundary conditions specific to the interface bonding for each case. In our system, the bottom face of the Sb film forms chemical bonds with the substrate surface. Since the film and the substrate are incommensurate, an accurate theoretical modeling including the substrate is not feasible. Instead, we simulate the effect of interfacial bonding by terminating the bottom face of a 4-BL Sb film with H. The results of the calculation, shown in Fig. 2(g), are in much better agreement with the experiment than the freestanding case. Specifically, the gap becomes zero, and the energy positions of the two surface bands are much closer to the

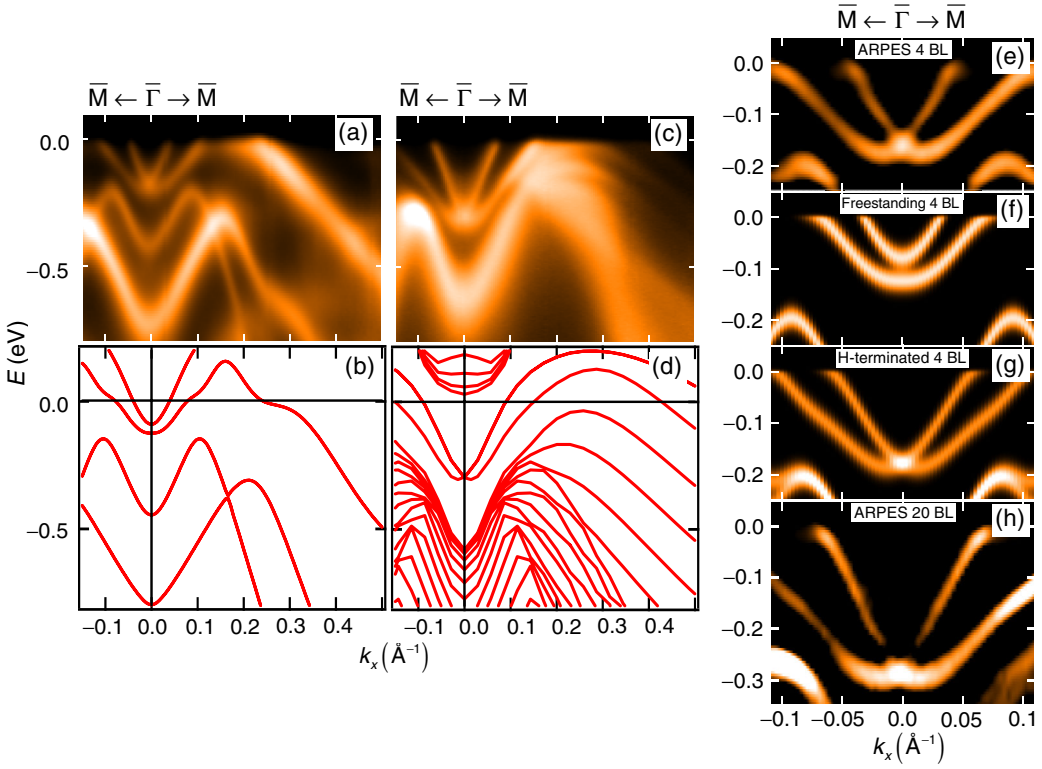

FIG. 2 (color online). (a) ARPES map for a 4-BL Sb film taken along the $\bar{\Gamma}$-$\bar{M}$ direction. (b) Calculated band structure of a 4-BL freestanding Sb film. (c) ARPES map for a 20-BL film. (d) Calculated band structure of a 20-BL freestanding Sb film. (e) Close-up view of the experimental surface band structure of a 4-BL film. The contrast has been enhanced by taking the second derivative along the energy axis. (f) Calculated band structure of a 4-BL film suitably broadened to simulate the data. (g) Same as (f) except that the bottom face of the film is terminated by H. (h) Close-up view of the experimental surface band structure of a 20-BL film.

experimental results. Thus, H termination is a good approximation for the interfacial bonding in our case. A similar case can be made for Bi termination [13]. For comparison, data from the 20-BL film, presented in Fig. 2(h), show no gap, just as expected. The surface states have somewhat lower energies, in agreement with the calculation shown in Fig. 2(d).

The absence of a gap at 4 BL can be understood as a result of the suppression of the tunneling-induced coupling. The chemical bonding at the interface introduces a large asymmetry in the film. The topological surface states at the interface undergo a large energy shift and are no longer degenerate with the surface states at the top surface. Quantum tunneling is thus turned off for lack of energy conservation, and the gap disappears correspondingly. This effect should become more pronounced at smaller film thicknesses. However, we have not been able to prepare atomically smooth films in the 1–3 BL range despite repeated attempts. Those films were rough probably due to an inherent critical thickness of 4 BL for smooth growth. Data at 5 BL confirm the lack of a gap [13].

To explore the nature of the tunneling interaction and interfacial coupling in detail, we show in Figs. 3(a) and 3(c), respectively, the calculated band dispersion relations for a freestanding 6-BL Sb film and for the same film with its bottom face terminated by H. For an intermediate case involving a weak interfacial bonding, we choose a model in which the bottom layer of the film is replaced by a mixture of Sb and Bi, represented in the calculation using the average pseudopotential of Sb and Bi. The rationale is that Sb and Bi are isoelectronic and chemically similar. The mixing is a good approximation for a somewhat perturbed bottom layer caused by a weak interfacial bonding. The results of the calculation are shown in Fig. 3(b). In Fig. 3(a), the two surface bands show a tunneling-induced gap. In Fig. 3(b), the surface states on the bottom face of the film are shifted slightly downward in energy by the interfacial perturbation, resulting in two separate Dirac cones at the zone center. In Fig. 3(c), the downward energy shift for the bottom surface states is so large that these states merge into the quantum-well manifold, and only the pair of top surface states remains in the gap with a zero gap at the Dirac point. The surface bands in Fig. 3(a) are doubly degenerate because of the two surfaces of the film, while those in Fig. 3(c) are nondegenerate.

The essential physics of the system can be further elaborated in terms of a four-band Rashba model with

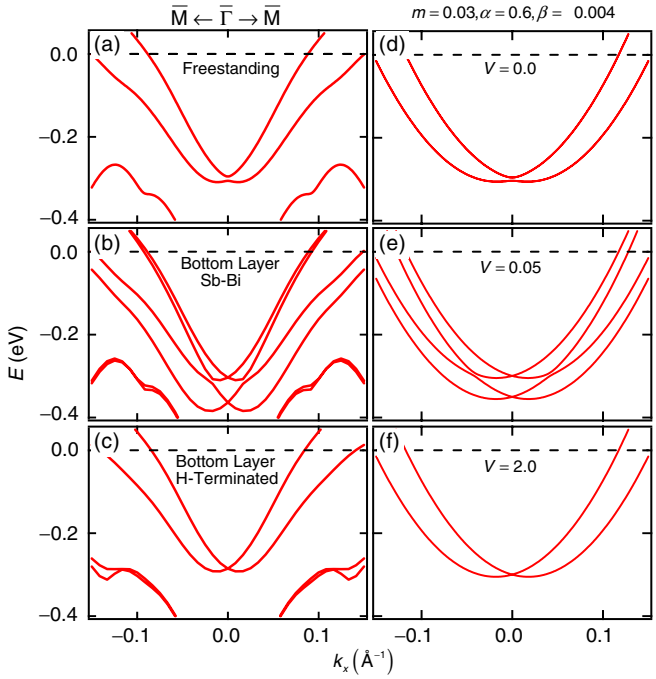

FIG. 3 (color online). Calculated band structure of a 6-BL Sb film with different bottom surface conditions: (a) freestanding, (b) bottom layer of Sb atoms replaced with Sb-Bi averaged pseudoatoms to simulate a weak interfacial bonding, and (c) bottom face terminated by H atoms. Also shown side-by-side for comparison are results of the four-band Rashba model with different surface biases: (d) $V = 0$, (e) $V = 0.05$, and (f) $V = 2.0$.

the basis set $\{|\Psi_T^{\uparrow}>, |\Psi_T^{\downarrow}>, |\Psi_B^{\uparrow}>, |\Psi_B^{\downarrow}>\}$, where Ψ is a surface state, and T and B denote the top and bottom surfaces, respectively. The effective Hamiltonian is

$$H(k) = \left(E_0 + \frac{k^2}{2m}\right)\mathbf{I}_4 + \alpha(k_x\sigma_y - k_y\sigma_x) \otimes \mathbf{I}_2 + \beta\mathbf{I}_2 \otimes \tau_x + V\mathbf{I}_2 \otimes \tau_z, \quad (1)$$

where $\mathbf{I}_n$ is an $n \times n$ identity matrix, $\boldsymbol{\sigma}$ and $\boldsymbol{\tau}$ are the Pauli matrices associated with the electron spin and position (top or bottom), respectively, α is the Rashba coupling constant, β is a (thickness-dependent) tunneling matrix element, and V is a potential bias exerted by interfacial bonding. A more general form of Eq. (1) might include a warping factor and higher-order band structure shape factors [21], but these are irrelevant to the present discussion. The calculated band structures with $m = 0.03$, $\alpha = 0.6$, $\beta = 0.004$, and $V = 0, 0.05$, and 2 in appropriate units (with energy in eV and momentum in Å^{-1}) are shown in Figs. 3(d)–3(f), respectively. The qualitative features of our findings thus far are well reproduced by the model. In particular, the tunneling-induced gap at $V = 0$, corresponding to a symmetric freestanding film, is eliminated at a large V, corresponding to a strong interfacial bonding.

The spin polarization of the surface states is a key property of concern for applications. It can be evaluated straightforwardly within the above model. The surface band dispersions for a fixed $\alpha = 0.6$ are shown in

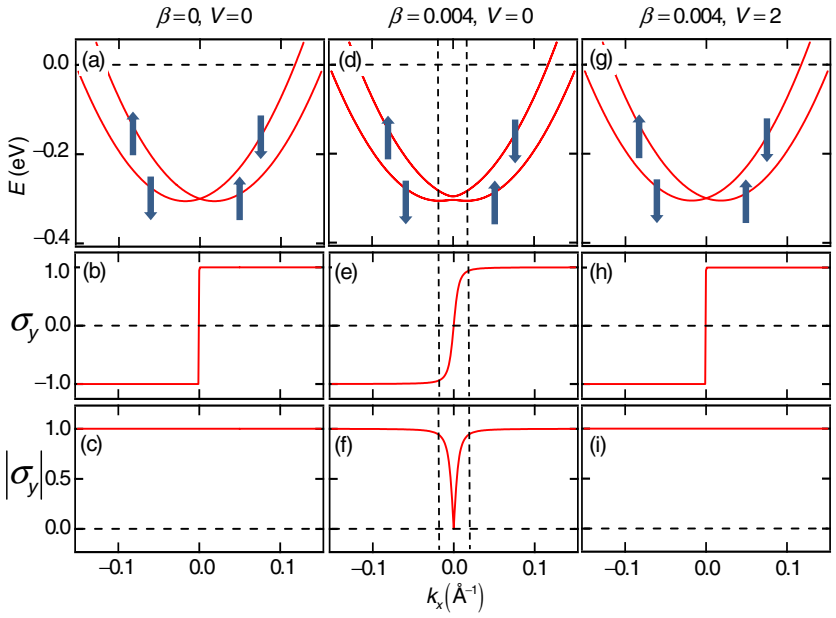

FIG. 4 (color online). (a) Band structure along k_x of the four-band Rashba model ($m = 0.03$ and $\alpha = 0.6$) with no tunneling ($\beta = 0$) and no surface bias ($V = 0$). (b) and (c) Normalized spin polarization and magnitude σ_y and $|\sigma_y|$, respectively, for the lower surface band. (d)–(f) Corresponding results for $\beta = 0.004$ and $V = 0$. (g)–(i) Corresponding results for $\beta = 0.004$ and $V = 2$.

Fig. 4 for (a) $\beta = 0$ and $V = 0$ (thick Sb sample with no tunneling), (d) $\beta = 0.004$ and $V = 0$ (6 BL freestanding film with quantum tunneling), and (g) $\beta = 0.004$ and $V = 2$ (6 BL film with strong interfacial bonding). Along $\bar{\Gamma} - \bar{M}$, the only nonzero component of the spin (in terms of the Pauli matrices) is σ_y. The values of σ_y and $|\sigma_y|$ for the lower surface band are shown in Fig. 4 for the three cases. In case (a), the system consists of a pair of chiral fermion bands and the electrons are fully spin polarized in accordance with the Rashba interaction. Each band undergoes a spin reversal as k_x crosses $\bar{\Gamma}$. In case (d), tunneling causes a gap to open up at the Dirac point. The magnitude of the spin is suppressed near $\bar{\Gamma}$, and the spin reversal becomes gradual. Thus, not only the insulating gap can cause problems for electrical transport, the suppression of the spin near the gap can be detrimental to spin transport. In case (g), the strong bonding at the interface restores the surface states and their spin properties to the thick-film limit, and the results appear identical to case (a). It should be noted that the 100% spin polarization based on this simple model is generally not realized in real materials because of the complex coupling of the spin and orbital degrees of freedom [22].

In conclusion, our ARPES mapping of the surface band structure of an ultrathin, atomically smooth, 4-BL Sb film prepared on a Bi-terminated Si(111)-$\sqrt{3} \times \sqrt{3} - R30°$ surface reveals no tunneling-induced energy gap at the Dirac point, despite a theoretically predicted one for a freestanding film. The observed robust Dirac cone, of interest to spintronic applications, is shown to be the result of a strong interfacial bonding between the film and the substrate, which suppresses quantum tunneling. Similar calculations performed for Bi_2Se_3 and Bi_2Te_3 films yield the same conclusions [13]. Our work suggests that quantum tunneling, an intrinsic property dependent on the film thickness, and substrate bonding, an extrinsic factor amenable to interfacial engineering, can be effectively manipulated to achieve desired electronic and spintronic properties of topological thin films.

This work is supported by the U.S. Department of Energy (Grant No. DE-FG02-07ER46383). The Synchrotron Radiation Center, where the ARPES data were taken, is primarily funded by the University of Wisconsin-Madison with supplemental support from facility users and the University of Wisconsin-Milwaukee. We acknowledge the U.S. National Science Foundation (Grant No. DMR-09-06444) and the U.S. Air Force Office of Scientific Research (Grant No. FA9550-09-1-030B) for partial support of the beam line operations. X. W. acknowledges financial support by the China Scholarship Council and the Young Scholar Plan of NJUST.

[1] M. Z. Hasan and C. L. Kane, Rev. Mod. Phys. **82**, 3045 (2010).
[2] X. L. Qi and S. C. Zhang, Rev. Mod. Phys. **83**, 1057 (2011).
[3] Y. A. Bychkov and E. I. Rashba, J. Phys. C **17**, 6039 (1984).
[4] Y. Li *et al.*, Adv. Mater. **22**, 4002 (2010).
[5] O. V. Yazyev, J. E. Moore, and S. G. Louie, Phys. Rev. Lett. **105**, 266806 (2010).
[6] A. C. Potter and P. A. Lee, Phys. Rev. Lett. **105**, 227003 (2010).
[7] D. Hsieh, Y. Xia, L. Wray, D. Qian, A. Pal, J. H. Dil, J. Osterwalder, F. Meier, G. Bihlmayer, C. L. Kane, Y. S. Hor, R. J. Cava, and M. Z. Hasan, Science **323**, 919 (2009).
[8] L. M. Falicov and P. J. Lin, Phys. Rev. **141**, 562 (1966).
[9] T. Kadono, K. Miyamoto, R. Nishimura, K. Kanomaru, S. Qiao, K. Shimada, H. Namatame, A. Kimura, and M. Taniguchi, Appl. Phys. Lett. **93**, 252107 (2008).
[10] K. Sugawara, T. Sato, S. Souma, T. Takahashi, M. Arai, and T. Sasaki, Phys. Rev. Lett. **96**, 046411 (2006).
[11] H. Höchst and C. R. Ast, J. Electron Spectrosc. Relat. Phenom. **137–140**, 441 (2004).
[12] G. Bian, T. Miller and T.-C. Chiang, Phys. Rev. Lett. **107**, 036802 (2011).
[13] See Supplemental Material at http://link.aps.org/supplemental/10.1103/PhysRevLett.108.176401 for additional information about the sample preparation procedures and the model calculations.
[14] J. M. Roesler, T. Miller, and T.-C. Chiang, Surf. Sci. Lett. **417**, L1143 (1998).
[15] I. Gierz, T. Suzuki, E. Frantzeskakis, S. Pons, S. Ostanin, A. Ernst, J. Henk, M. Grioni, K. Kern, and C. R. Ast, Phys. Rev. Lett. **103**, 046803 (2009).
[16] X. Gonze *et al.*, Comput. Mater. Sci. **25**, 478 (2002).
[17] X. Gonze *et al.*, Z. Kristallogr. **220**, 558 (2005).
[18] C. Hartwigsen, S. Goedecker, and J. Hutter, Phys. Rev. B **58**, 3641 (1998).
[19] T.-C. Chiang, Surf. Sci. Rep. **39**, 181 (2000).
[20] Y. Zhang *et al.*, Nature Phys. **6**, 584 (2010).
[21] L. Fu, Phys. Rev. Lett. **103**, 266801 (2009).
[22] G. Bian, X. Wang, Y. Liu, T. Miller, and T.-C. Chiang, Phys. Rev. B **84**, 235414 (2011).